minerals

MDPI

Article

Radiological Risk Parameters of the Phosphorite Deposits, Gebel Qulu El Sabaya: Natural Radioactivity and Geochemical Characteristics

El Saeed R. Lasheen [1,*], Hesham M. H. Zakaly [2,3], B. M. Alotaibi [4], Diaa A. Saadawi [1], Antoaneta Ene [5,*], Douaa Fathy [6], Hamdy A. Awad [7] and Raafat M. El Attar [8]

1 Geology Department, Faculty of Science, Al-Azhar University, Cairo 11884, Egypt
2 Institute of Physics and Technology, Ural Federal University, 620002 Yekaterinburg, Russia
3 Physics Department, Faculty of Science, Al-Azhar University, Assiut Branch, Assiut 71524, Egypt
4 Department of Physics, College of Science, Princess Nourah Bint Abdulrahman University, P.O. Box 84428, Riyadh 11671, Saudi Arabia
5 Department of Chemistry, Physics, and Environment, Faculty of Sciences and Environment, INPOLDE Research Center, Dunarea de Jos University of Galati, 47 Domneasca Street, 800008 Galati, Romania
6 Geology Department, Faculty of Science, Minia University, El-Minia 61519, Egypt
7 Geology Department, Faculty of Science, Al-Azhar University, Assiut Branch, Assiut 71524, Egypt
8 Geology Department, Faculty of Science, South Valley University, Qena 83523, Egypt
* Correspondence: elsaeedlasheen@azhar.edu.eg (E.S.R.L.); antoaneta.ene@ugal.ro (A.E.)

Citation: Lasheen, E.S.R.; Zakaly, H.M.H.; Alotaibi, B.M.; Saadawi, D.A.; Ene, A.; Fathy, D.; Awad, H.A.; El Attar, R.M. Radiological Risk Parameters of the Phosphorite Deposits, Gebel Qulu El Sabaya: Natural Radioactivity and Geochemical Characteristics. *Minerals* **2022**, *12*, 1385. https://doi.org/10.3390/min12111385

Academic Editors: Manuel Jesús Gázquez and Juan Pedro Bolívar Raya

Received: 22 August 2022
Accepted: 28 October 2022
Published: 30 October 2022

Abstract: This study investigates the distribution of natural radioactivity and geological, geochemical, and environmental risk assessments of phosphorite deposits to determine their suitability for international applications (such as phosphoric acid and phosphatic fertilizers). The examined Late Cretaceous phosphorite deposits belong to the Duwi Formation, which is well exposed on the southern scarp boundary at the central part of Abu Tartur Plateau, Gebel Qulu El Sabaya, East Dakhla Oasis. This formation is classified into lower phosphorite, middle shale, and upper phosphorite members. The lower phosphorite ranges in thickness from 2 to 3.5 m and mainly comprises apatite (possibly francolite), dolomite, calcite, quartz, hematite, anhydrite, and kaolinite. They contain an average concentration of CaO (38.35 wt.%), P_2O_5 (24.92 wt.%), SiO_2 (7.19 wt.%), Fe_2O_3 (4.18 wt.%), MgO (3.99 wt.%), F (1.59 wt.%), Al_2O_3 (1.84 wt.%), Na_2O (1.33 wt.%), and K_2O (0.22 wt.%). Natural radioactivity and radiological parameters were investigated for fifteen samples of phosphorites using a NaI (Tl) scintillation detector. Absorbed dose rates, outdoor and indoor annual effective dose, radium equivalent activity, external and internal hazard, and excess cancer risk values are higher than the recommended levels, reflecting that exposure to these deposits for a long time may lead to health risks to human organs.

Keywords: Gebel Qulu El Sabaya; Duwi Formation; phosphorite; radiological health; radioactivity

1. Introduction

The sedimentary, igneous, and metamorphic rocks are widely distributed and cover vast areas of the Egyptian Sinai, Eastern, and Western Deserts [1–7]. Egyptian phosphorite deposits belong to the Duwi Formation as a part of the Mediterranean phosphorite belt, which extends from the African (west) to the Asian (east) Arab countries. Egyptian phosphorite occurrences are subdivided by [8] into three belts, east-west trending. The economic occurrences are restricted to the central facies belt, confined to the following localities, the Red Sea coast from Safaga to Quseir; the Nile Valley between Idfu and Qena; and the Western Desert between Kharga and Dakhla oases (Abu Tartur area). The Phosphorite (Duwi) Formation is conformably overlain by the Dakhla Formation and is assigned to Upper Campanian to Early Maastrichtian age [8–11]. In the present study, the Gebel Qulu El Sabaya sector is extended east-west for about 13 km along the southern scarp boundary

at the central part of Abu Tartur Plateau, located about 15 km north of the Dakhla–Kharga road (Figure 1).

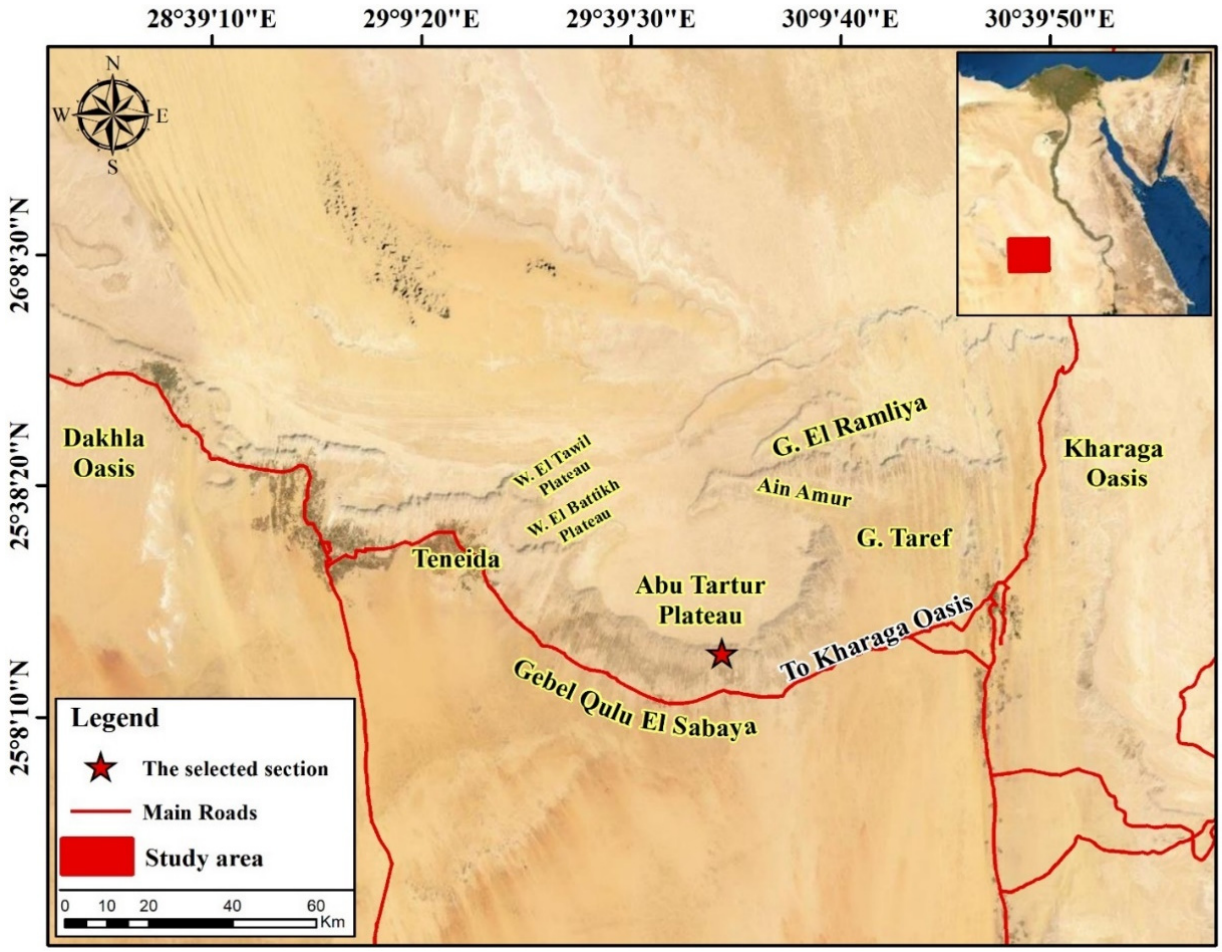

Figure 1. Location map of the studied Gebel Qulu El Sabaya, East Dakhla Oasis.

In general, the lithostratigraphic section of Gebel Qulu El Sabaya is based on the Quseir shale Member of the Nubia Formation, overlain by the Duwi Formation and Dakhla Formation at the top. The Duwi Formation comprises three members; the lower one is the productive phosphorite. The lower member of the Duwi Formation in the Abu Tartur area represents a productive phosphorite bed with a thickness ranging from 0.7 up to 10 m, while the middle member is composed of black shale and siltstone with a thickness ranging from 12 to 28 m [12]. On the other hand, the upper member has three thin phosphatic bands intercalated with black shale with a total thickness ranging from 0.7 to 1 m. The Duwi Formation is unconformably overlying the Quseir shale member with an undulating surface where the non-oxidized phosphorite rocks were deposited in a reducing environment and changed to a yellowish-brown color by subsequent chemical oxidation processes [13,14]. The geochemistry of phosphorites and their main mineral constituent, francolite, have been widely studied due to their economic importance. Variability in the chemical composition of francolite may reflect the difference in original composition and modification during diagenesis [15]. All sedimentary phosphorites, everywhere in the world, are mainly composed of carbonate fluorapatite (traditionally known as francolite), but the fluorine content increases with age.

The phosphorite rocks were considered a natural source of uranium, where the uranium-bearing minerals were formed in the sedimentary phosphorite during deposition and digenesis by the seawater. Apatite is a common mineral that contains high

concentrations of uranium, which range from 30 to 300 ppm, and may reach up to 500 ppm in phosphorite reworked in the marine environment. The main uranium components in phosphorite are U^{+4} and U^{+6}. The tetravalent form is partially replaced by Ca^{+2} in the apatite lattice because of their similar ionic radii, while the hexavalent one is enriched in the ore by adsorption onto the mineral surface [16]. Abu Tartur phosphorite contains the highest recorded concentration of REEs (up to 2000 ppm) [17]. They stated that the Abu Tartur phosphorite has the lowest uranium content at about 24 ppm, relative to El Sibaiya phosphorite at 85 ppm and the Red Sea phosphorite at 68 ppm. The rare earth elements (REEs) patterns of marine phosphorite are useful indicators of marine depositional environments [18]. However, REEs signatures can be altered by burial digenesis or by surface weathering [19].

This study deals with stratigraphical, petrographical, mineralogical, and geochemical investigations of the lower phosphorite member of the Duwi Formation at Gebel Qulu El Sabaya in order to identify the thickness and principal constituents of this phosphorite member. In addition, natural radioactivity and radiological parameters were applied to deduce their impact on human organs.

2. Materials and Methods

2.1. Geological Setting

The Western Desert covers more than 65% of Egypt, spreading from the Nile Valley to the Libyan border. It is a plateau desert with several oases, including Kharga, Farafra, Dakhla, and Beris. It initially developed during the Neotethys opening in the Late Triassic and Early Jurassic periods.

Phosphorite beds are exposed in the stratigraphic section of Gebel Qulu El Sabaya. Herein, the Duwi Formation unconformably overlies the Campanian variegated Quseir shale member of the Nubia Formation with undulating erosion contacts and is conformably overlain by the marine laminated Maestrichtian grey to black shale and marls of the Dakhla Formation (Figure 2). The Duwi Formation is made up of coarse-fine phosphorite grains intercalated with dolomitic phosphorite, glauconitic shale, and black shale lenses in the lower part and glauconitic shale in the middle, with hard dolomitic phosphorite beds intercalated with black shale bands in the upper part. An undulating surface and conglomerate bed characterize the unconformable boundary between the Quseir Member and the overlying Duwi Formation, like the Abu Tartur area [13,14]. The Duwi Formation in the studied area is classified after Issawi et al. [9,10] and [14] into lower phosphorite (I), middle shale (II), and upper phosphorite (III) members (Figure 2).

The lower phosphorite member consists of moderately hard oxidized phosphorite of yellowish-brown color intercalated with black shale lenses with an average thickness of 0.4 m. The total thickness of this member ranges from 2 to 3.5 m with an average of 2.5 m, which could be considered the economic phosphorite beds in the studied area (Figure 2).

The middle shale member is mainly composed of glauconitic shale, siltstone, and grey shale, characterized by cracking filled with gypsum and ferruginous staining. This member has a thickness range of 0.3 to 1.1 m with an average of 0.8 m (Figure 2).

The upper phosphorite member comprises hard dolomitic phosphate beds intercalated with grey-to-black shale lenses. Its thickness varies from 0.2 to 0.3 m, with an average of 0.25 m (Figure 2).

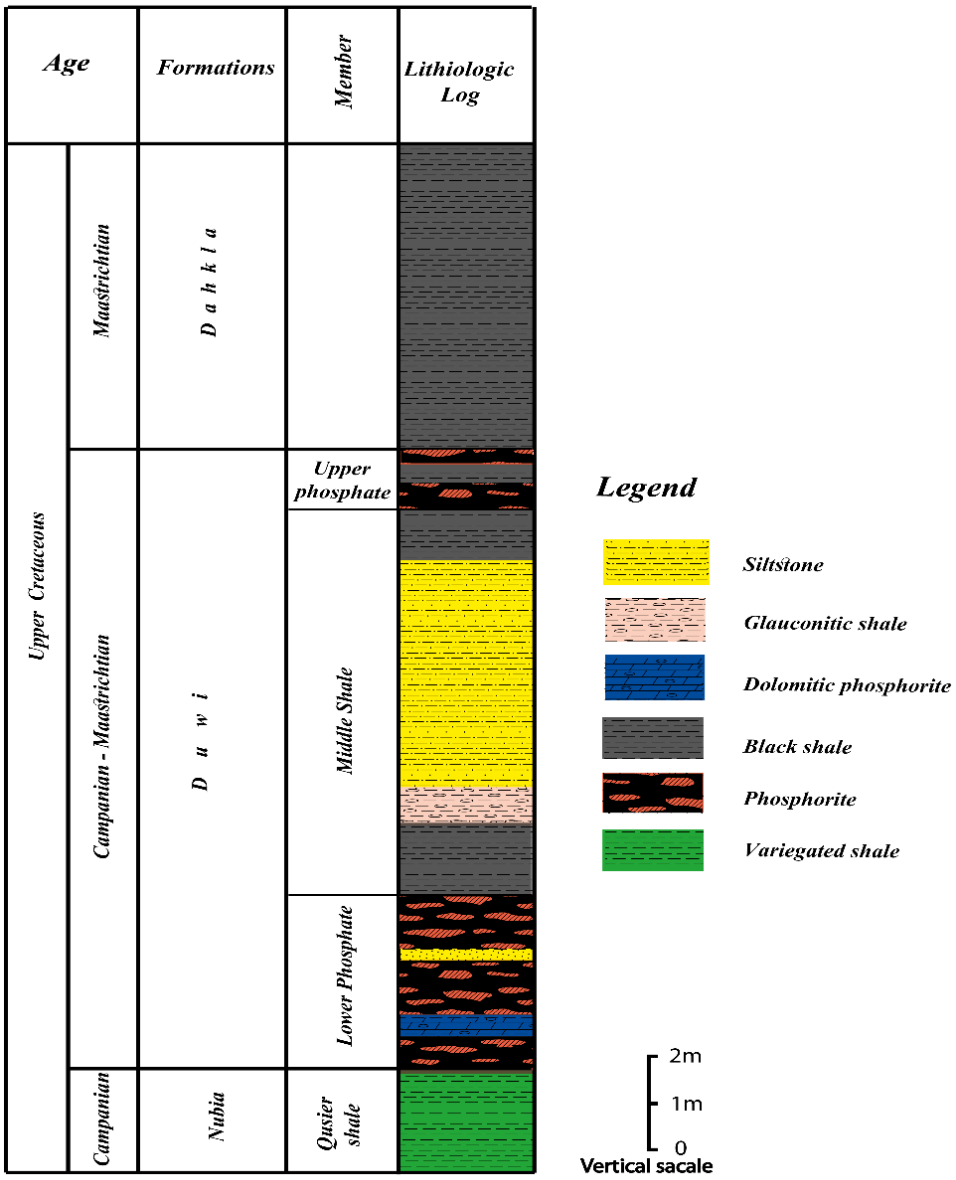

Figure 2. The general lithostratigraphic section of exposed rock units at Gebel Qulu El Sabaya, the southern scarp in the central part of the Abu Tartur Plateau.

2.2. Petrography

The investigated phosphorite samples of the Gebel Qulu El Sabaya area microscopically show two principal constituents: phosphatic components (apatite, fish bone fragments, and shark teeth) and non-phosphatic components (dolomite, calcite, and iron oxides) as cement materials (Figure 3). The phosphate grains are generally angular to sub-rounded, elongated in shape, and yellowish brown in color (Figure 3a,b,d), which could be reflective of the effect of oxidation of pyrite mineral and the formation of iron oxyhydroxides [14].

Fishbone fragments are generally elongated to sub-angular in shape (Figure 3b). Bone fragments and teeth of different sizes and shapes are common as clastic allelochemical constituents. On the other hand, the non-phosphate cementing components are mostly composed of microcrystalline dolomite, glauconite, calcite grains, and iron oxides (Figure 3b,c). The replacement of phosphate grains by cementing material (dolomite rhombus) reflects the digenetic process effect (Figure 3c).

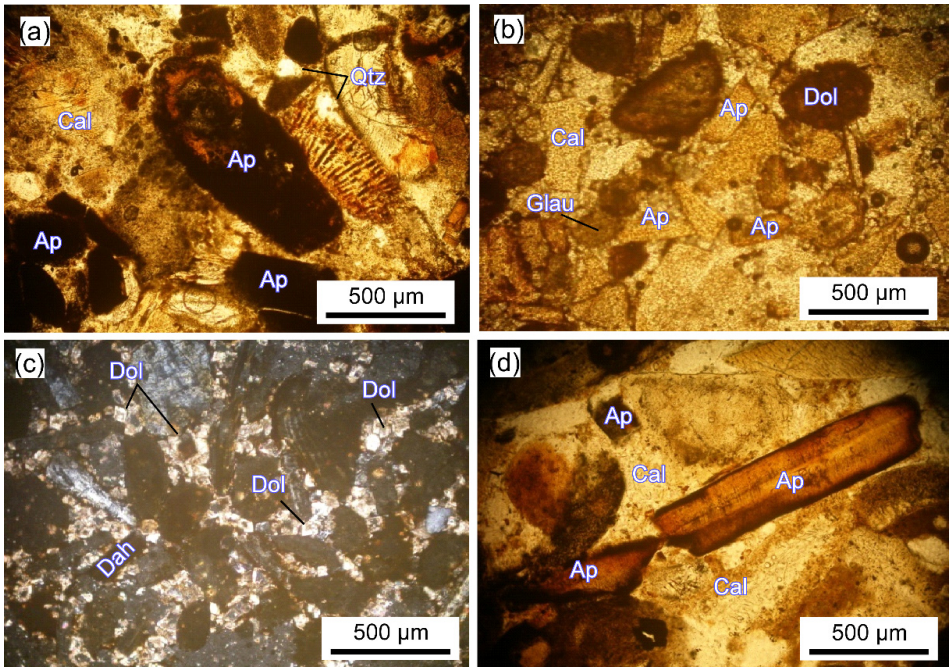

Figure 3. Photomicrographs showing (**a**) Apatite (Ap) grains with bone fragments embedded in calcite (Cal) and silica (Qtz) matrix; (**b**) Apatite grains elongated to surrounded with bone fragments and shark teeth, glauconite (Gaul), and dolomite (Dol) embedded in carbonate cement; (**c**) Dahlite (Dah) and dolomite grains with bone fragments embedded in carbonate cement; and (**d**) Elongated apatite (Ap) grains with bone fragments embedded in carbonate cement.

2.3. Sampling and Analytical Techniques

Fifteen representative samples were collected from Gebel Qulu El Sabaya sections to cover most of the lower phosphorite members at Gebel Qulu El Sabaya. The petrographic characteristics were microscopically investigated for five representative samples. These samples were prepared and subjected to complete wet chemical analysis to estimate their major oxides. At the same time, the trace elements were measured using an XRF (X-ray fluorescence) Philips X-ray spectrometer in the laboratories of the Nuclear Materials Authority. Rare earth elements (REEs) were analyzed using induced Couple Plasma (ICP). The concentrations of uranium (ppm), thorium (ppm), radium (ppm), and potassium (%) in different rock types were detected γ-spectrometric by using a multi-channel analyzer with a 76 $\times$ 76 mm NaI detector [20]. These samples are grinded and preserved in plastic containers for at least 21 days to accumulate free radon and other isotope emissions. The stability spectrometer channels change due to variations in power supply and amplification of the photomultiplier tube.

An empty sealed beaker with the same geometry as the samples was used to evaluate the background around the detector. With 12 h of measurement time, the Genie 2000 (Canberra) software was used to analyze the spectrum. The ^{226}Ra activity was evaluated using γ-peaks of ^{214}Pb (0.3519 MeV (36.7%)) and of ^{214}Bi (0.6093 MeV (46.1%), 1.1203 MeV (15%), 1.7286 MeV (3.05%), and 1.764 MeV (15.9%)). The ^{232}Th activity was estimated using γ-peaks of ^{228}Ac (0.9112 MeV (29%)), ^{212}Pb (0.2386 MeV (43.6%)), and ^{208}Tl (0.5831 MeV (84.5%). The ^{40}K activity was estimated using a self γ-peak of 1.461 MeV (10.7%).

2.4. Energy and Efficiency Calibration

Variations influence the stability of the energy of the spectrometer channels in the power supply, voltage, and photomultiplier tube amplification characteristics. The characteristics of the power supply and the photomultiplier are impacted by temperature. To ensure that the instrument accurately records the gamma radiation energy of the radioactive elements, a permanent calibration is performed using radioactive calibration sources like

^{137}C (made in channel 662) and ^{57}Co (122.1 keV, manufactured in channel 122): First, the ^{137}Cs source is used for gain adjustments before the ^{57}Co source is used for zero alterations, and second, the ^{137}Cs source is usually used as a minimum technique.

The efficiencies was estimated experimentally using standard sources (IAEA-314) with particular activity for Radium-226 (732 Bqkg^{-1}) and Thorium-232 (17.8 ppm). According to an academic program in MATLAB, the absolute efficiency at any interesting energy varied from 10 to 1764 keV. For Quality Assurance, the uncertainty of activity u(A) was evaluated using the following formula.

$$u(A) = A\sqrt{[\frac{u(N_p)}{N_p}]^2+[\frac{u(\eta)}{\eta}]^2 + [\frac{u(m)}{m}]^2+[\frac{u(P\gamma)}{P\gamma}]^2}$$

where $u(Np)$, $u(\eta)$, $u(m)$, and $u(P\gamma)$, respectively, stand for the absolute efficiency for each gamma line discovered in the same number of channels in the sample, sample mass, and absolute transition probability of decay. Computer "analysis" software calculated the uncertainty of each individual net-peak area.

3. Results and Discussion

3.1. Geochemical Characteristics

3.1.1. Major Oxides

The collected phosphorite samples of the Gebel Qulu El Sabaya area were subjected to chemical analysis to determine the content of the major oxide (Table 1 and Figure 4). Results show that the studied phosphorite deposits are dominated by CaO (36–41 wt.% with an average of 38.35 wt.%), P_2O_5 (22–27.4 wt.% with an average of 24.92 wt.%), SiO_2 (5.4–9.2 wt.% with an average of 7.19 wt.%), MgO (3–3.4 wt.% with an average of 3.99 wt.%), and Fe_2O_3 (3–4.8 wt.% with an average of 4.18 wt.%).

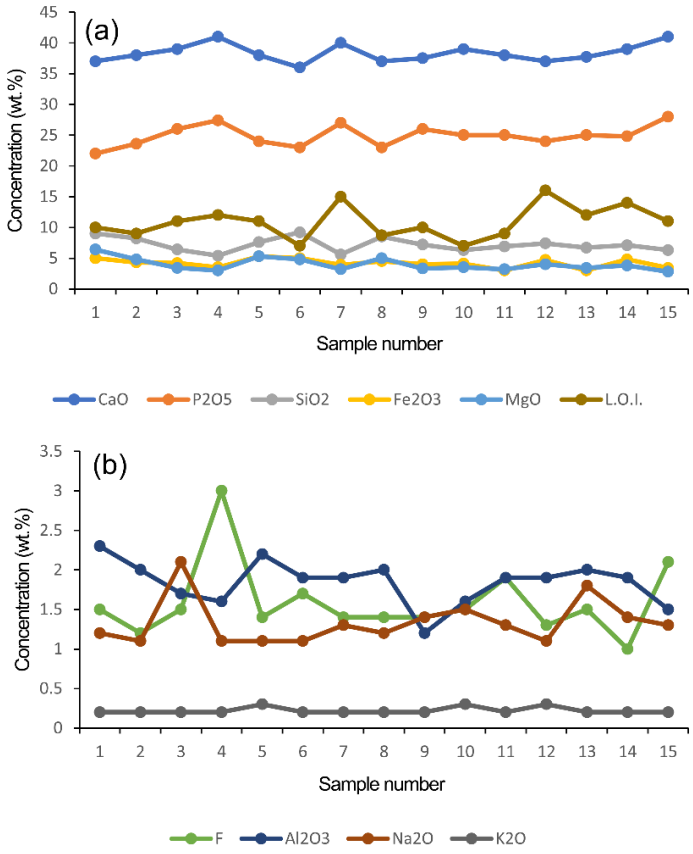

Figure 4. (**a**,**b**) Distribution curves of the major oxides (wt.%) in phosphorite samples.

Table 1. Whole rock {major (wt.%), trace (ppm), and REEs (ppm)} analysis of Gebel Qulu El Sabaya phosphorite samples.

S.NO.	1	2	3	4	5	6	7	8	9	10	11	12	13	14	15
CaO	37	38	39	41	38	36	40	37	38	39	38	37	38	39	41
P_2O_5	22	24	26	27	24	23	27	23	26	25	25	24	25	25	28
SiO_2	9	8	6	5	8	9	6	9	7	6	7	7	7	7	6
Fe_2O_3	5	4	4	4	5	5	4	5	4	4	3	5	3	5	3
MgO	6	5	3	3	5	5	3	5	3	4	3	4	3	4	3
F	2	1	2	3	1	2	1	1	1	2	2	1	2	1	2
Al_2O_3	2	2	2	2	2	2	2	2	1	2	2	2	2	2	2
Na_2O	1	1	2	1	1	1	1	1	1	2	1	1	2	1	1
K_2O	0	0	0	0	0	0	0	0	0	0	0	0	0	0	0
L.O.I.	10	9	11	12	11	7	15	9	10	7	9	16	12	14	11
Cd	12	11	9	10	8	11	7	5	4	8	7	11	9	14	18
Cr	111	113	75	91	153	145	93	76	141	77	98	113	122	157	114
Cu	30	33	32	29	27	28	24	10	26	29	26	27	11	19	24
Ni	41	47	39	40	42	44	43	12	44	39	43	45	18	42	39
Zn	73	198	159	156	158	149	152	69	127	95	157	201	143	179	181
Pb	2	6	10	9	5	7	3	2	6	11	3	6	3	9	12
U	33	29	35	35	30	26	22	27	36	24	27	29	32	30	28
Y	615	611	265	236	228	217	211	255	100	218	268.	548	603	611	605
La	240	208	285	301	276	271	247	161	83	298	280	221	254	250	216
Ce	554	549	543	533	543	555	535	540	540	526	542	546	552	550	549
Pr	45	55	63	55	62	64	45	66	48	55	64	53	54	46	54
Nd	288	273	283	220	298	218	290	215	230	283	280	268	283	285	258
Sm	85	118	90	60	87	56	63	51	54	45	55	42	130	77	84
Eu	18	15	10	18	15	18	10	12	18	17	15	18	15	18	10
Gd	75	78	70	81	78	76	79	75	68	93	88	78	82	73	78
Tb	7	5	9	5	8	5	9	5	8	7	5	7	5	9	8
Dy	65	58	65	78	60	85	53	48	65	65	63	68	73	78	70
Ho	5	5	5	8	5	8	8	5	8	5	5	5	5	8	5
Er	33	25	35	28	30	35	33	38	33	43	27	28	40	37	35
Tm	5	5	3	8	5	8	8	5	8	3	5	10	5	8	5
Yb	41	42	38	35	45	38	33	38	34	33	35	40	37	33	32
Lu	3	5	3	7	3	8	3	9	3	7	3	9	3	8	5
TREEs	1464	1441	1502	1437	1515	1445	1416	1268	1200	1480	1467	1393	1538	1480	1409

The average content of Al_2O_3 and F is 1.84 wt.% and 1.59 wt.%, respectively. However, Na_2O and K_2O are minor constituents, showing averages of 1.33 wt.% and 0.22 wt.%, respectively. Traditionally, CaO and P_2O_5 are the main components of apatite minerals, while Fe_2O_3 and MgO content is related to the presence of hematite and dolomite minerals, respectively. On the other hand, the observed variation in the P_2O_5 content from one sample to another (22–27.4 wt.% P_2O_5) could reflect the digenetic and geochemical processes that cause limited replacement of P_2O_5 by other components such as SiO_2, MgO, and Fe_2O_3. The microscopic examination indicated the replacement of phosphate particles by cementing materials. This reduces the grade of the phosphorite. Generally, the P_2O_5, Fe_2O_3, and MgO contents are widely used for quality evaluation in the industry.

Phosphorite ore deposits into three grades: high (with more than 27 wt.% of P_2O_5), medium (27 to 23 wt.% P_2O_5), and low (with less than 23 wt.% of P_2O_5) [21]. According to that classification, the studied phosphorite of Gebel Qulu El Sabaya is considered a medium grade (an average of 24.92 wt.% P_2O_5). This phosphorite, compared with other Egyptian phosphorites, is nearly similar in P_2O_5 relative to Abu Tartur [12] and Sibaiya phosphorites according to [22] and higher in Fe_2O_3 and MgO content (Table 2). This variation may be due to a slight difference in the depositional environment or geochemical process.

Table 2. Comparison of the examined major oxides (wt.%) of Qulu El Sabaya phosphorites with some Egyptian phosphorites.

Areas	CaO	P_2O_5	SiO_2	Fe_2O_3	MgO	Al_2O_3	Na_2O	K_2O
Gebel Qulu El Sabaya (present study)	38.35	24.92	7.19	4.18	3.99	1.84	1.33	0.22
El Ziat phosphorite [19]	38.72	24.75	7.3	3.38	3.4	1.7	0.92	0.2
Eldehous phosphorites [10]	35.3	22.7	10.6	4.8	6.9	1.9	1.8	0.2
Abu Tartur [13]	40	25	5	3	3	2	0.6	0.14
Sibaiya Phosphorite [13]	36	25	18	2.23	2.4	1.79	0.88	0.22

3.1.2. Trace Elements

The concentration of trace elements in Gebel Qulu El Sabaya phosphorite samples is shown in (Table 1, Figure 5a). Cd (ranges from 4 ppm to 18 ppm with an average of 10 ppm), Cr (from 75 ppm to 757 ppm, avg. = 112 ppm), Pb (2–12 ppm, avg. = 6 ppm), Cu (10–33 ppm; avg. = 25 ppm), and Ni (18–47 ppm, avg. = 39 ppm). They reveal a wide variation, particularly in Zn content, in the studied phosphorite samples, ranging from 69 ppm to 201 ppm with an average of 146 ppm. Zn content is attributed to the presence of the sulfate phase in phosphorites [23].

3.1.3. Rare Earth Elements (REEs)

The geochemistry and economic importance of REEs in the Western Desert phosphorite were first considered by El-Kammar [24], who reported REEs abnormality in Abu Tartur phosphorite. Then, Dardir and Kobtan [25] reported on the economic potentiality of REEs in Abu Tartur phosphorite (about 1718 gm/ton, on average). Amin and Zidan [17] stated that the average REEs content in Abu Tartur phosphorite is 2000 ppm. In addition, REEs contained in phosphorite may be extracted as a by-product during phosphoric acid production [13]. Gebel Qulu El Sabaya phosphorite samples exhibit total REEs content ranging from 1200 to 1538 ppm with an average of 1430 ppm (Table 1). Furthermore, the increase in REEs concentration from the west to east is most likely related to depositional and diagenetic factors. On the other hand, the average total REEs content recorded in the studied phosphorite is nearly like that of Abu Tartur phosphorite at 1407 ppm [25] and higher than that recorded in Eldehous phosphorite at 616 ppm [26].

Normalization of REEs to the Post Archean Australian Shale (PASS) values [27] is shown in Figure 5b. The normalized REE pattern shows that the Gebel Qulu El Sabaya phosphorite is characterized by a slight negative Eu anomaly (Figure 5b). El-Kammar and El-Kammar [28] stated that the Dakhla phosphorite could generally be described as Ce and Eu deficit. Additionally, the plots show that Gebel Qulu El Sabaya phosphorites have a very similar REEs pattern to Abu Tartur phosphorites (Figure 5b). This non-conventional distribution is not comparable to seawater and many other marine phosphorites, characterized by large negative Ce anomalies [29–34].

Accordingly, the authors believe that seawater is not the only ultimate source of REEs in the studied phosphorite. This behavior could be related to the influence of heavy detrital minerals like monazite admixed with the studied phosphorite. Similar behavior was previously described in East Sibaiya phosphorite [35] and Gabal Tarawan phosphorite of Kharga Oasis [26]. Hassan and El-Kammar [36] stated that the shallow nature of the depositional basin of Abu Tartur phosphorite maintained a higher influx of heavy detrital minerals than other Egyptian phosphorites. They added that this case seems to apply to most Western Desert phosphorites.

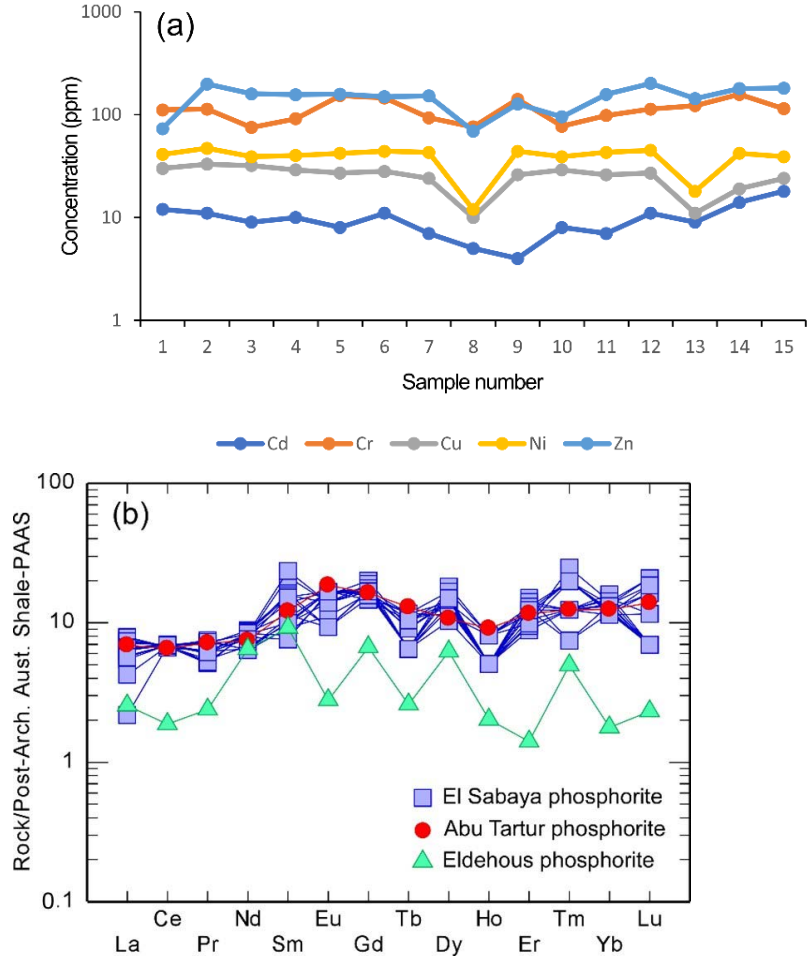

Figure 5. (**a**) Trace elements distribution curves of the examined phosphorite samples; and (**b**) REEs-normalized to Post Archean Australian Shale (PASS) [27] of the examined phosphorite and compared with the average REEs of Abu Tartur phosphorite [25] and Eldehous phosphorite [26].

3.2. Radioactivity Concentrations

Radiometrically, it is found that the equivalent uranium content (eU) in Gebel Qulu El Sabaya phosphorite ranges from 28 ppm to 42 ppm with an average of 36 ppm, which is slightly higher than the chemical uranium (cU), which attains values ranging between 22 ppm and 36 ppm with an average of 30 ppm. However, the Ra content ranges from 33 to 44 ppm with an average of 38.4 ppm (Table 3). Uranium enrichment in phosphorite may be ascribed to apatite lattice and/or adsorbed on the cement [37]. The geochemical relations of U with some major and trace elements of Sinai phosphates mentioned that U is associated with carbonate-apatite and was derived from seawater (i.e., syngenetic origin) [38]. The average radiometric uranium content of the studied phosphorite at 35 ppm is higher than that of El Ziat phosphorite (27 ppm) [19] and Abu Tartur phosphorite (23 ppm) [13]. On the contrary, it is lower than those of Sibaiya phosphorites [13], Red Sea phosphorites [13], and Morocco phosphorites [20]. The eU/eTh ratio is widely used as a geochemical indicator for uranium migration and re-mobilization. This ratio ranges from 4–42, reflecting a high degree of uranium mobilization. In addition, P-factor (eU/Ra) [39] as well as D-factor (Uc/eU) [40] are used for uranium migration and re-mobilization. eU/Ra and Uc/eU ratios of the examined phosphorites are less than unity (avg. = 93 and 0.83, respectively), reflecting the removal of uranium. However, uranium mobilization can be calculated using the [41] equation (eUm = eU-eTh/3.5). The results are more than one (av. 9.81), suggesting U enrichment. ^{238}U, ^{232}Th, ^{226}Ra, and ^{40}K (Bq/kg) activity concentrations for the examined Qulu El Sabaya phosphorites are given in Figure 6. This figure reveals the measured activity

concentrations (Bq/kg) of 15 samples that were measured radiometrically using the NaI technique. It is noticeable that the studied rocks show a wide variation in their ^{238}U (av. 462.93 ± 55.76 Bq/kg), ^{232}Th (av. 12.12 ± 3.3 Bq/kg), and ^{226}Ra (av. 432.9 ± 47.96 Bq/kg) concentrations, which are higher than the recommended values of UNSCAR [42,43].

Table 3. Radiometric measurements (ppm) of the examined phosphorites compared with other phosphorites.

S.NO.	eU	eTh	eRa	eU/eTh	eU/eRa	cU/eU	cU
1	39	1	40	39	1	1	33
2	40	5	41	8	1	1	29
3	41	6	44	7	1	1	35
4	31	4	33	8	1	1	35
5	32	5	38	6	1	1	30
6	32	8	37	4	1	1	26
7	31	2	36	16	1	1	22
8	35	7	36	5	1	1	27
9	42	1	44	42	1	1	36
10	28	2	33	14	1	1	24
11	38	1	39	38	1	1	27
12	36	5	38	7	1	1	29
13	31	4	33	8	1	1	32
14	41	3	43	14	1	1	30
15	40	2	41	20	1	1	28
Min.	28	1	33	4	1	1	22
Max.	42	8	44	42	1	1	36
Average	36	4	38	16	1	1	30
El Ziat phosphorite [19]	27	-	25	-	-	-	-
Eldehous phosphorites [10]	35	-	35	-	-	-	-
Abu Tartur phosphorites [13]	23	-	19	-	-	-	-
Sibaiya phosphorites [13]	85	-	89	-	-	-	-
Red Sea phosphorites [13])	68	-	69	-	-	-	-

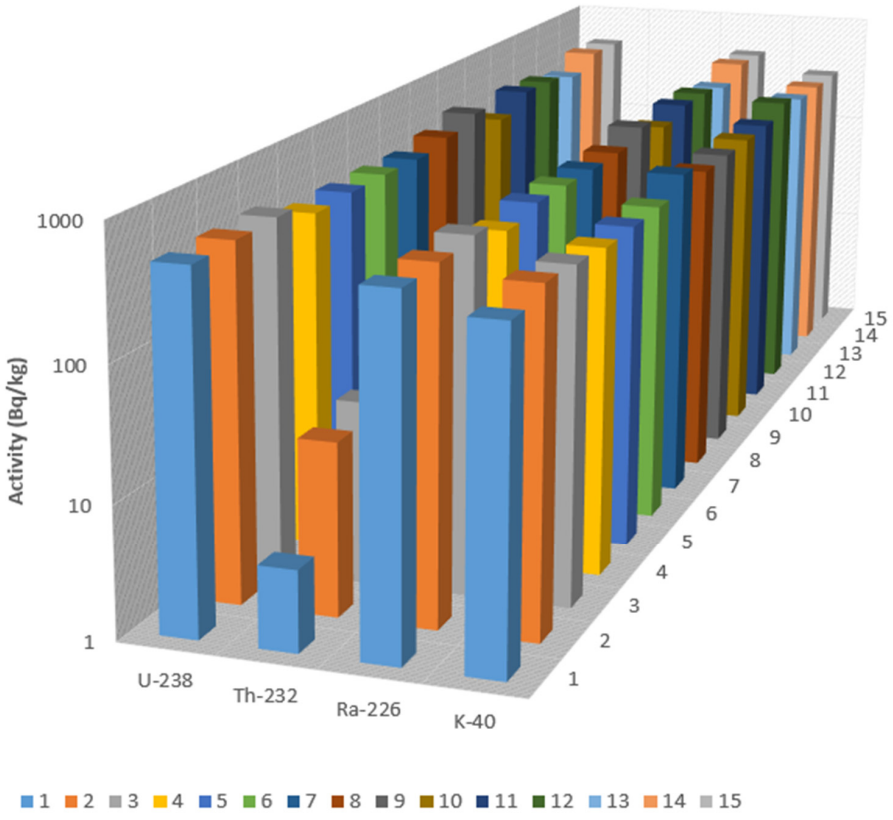

Figure 6. The samples represent the radiometric measurements of ^{238}U, ^{226}Ra, ^{232}Th, and ^{40}K (Bq/Kg).

3.3. Radiological Risk Parameters

From ^{238}U, ^{232}Th, ^{226}Ra, and ^{40}K (Bq/kg) activity concentrations for the examined Qulu El Sabaya phosphorites, we computed the radiological hazards indices given in Table 4. This table reveals the computed radiological hazards, minimum, maximum, mean, and standard deviation of 15 samples that were measured radiometrically using the NaI technique. The distribution frequency histogram of rocks under investigation was determined by analyzing all related radionuclides (^{238}U, ^{226}Ra, and ^{232}Th; Figure 7). The frequency distributions of activity concentration of all the radionuclides were analyzed, and the histograms are given in Figure 7. The ^{226}Ra, ^{232}Th, and ^{40}K graphs show that these radionuclides demonstrate a normal (bell-shape) distribution. Without a degree of multi-modality. This multi-modal feature of the radioelements demonstrates the complexity of Gebel Qulu El Sabaya samples.

Radiological risk parameters were calculated for Qulu El Sabaya in order to infer the radiation effect on human organs during extraction or mining processes. These assessments include absorbed gamma dose, annual (outdoor and indoor) effective dose, radium equivalent activity, external and internal hazard indices, and excess cancer risk (Table 4).

Absorbed gamma-dose rate (D_{air})

The absorbed gamma-dose rate was used to assess the gamma rays that were released >1 m from the Earth's surface [42,43]. ^{238}U, ^{232}Th, and ^{40}K activity concentrations are used to estimate the D_{air} as the following:

$$D_{air}\ (nGy/h) = 0.430\ U + 0.666\ Th + 0.042\ K \quad (1)$$

where Th, U, and K are ^{232}Th, ^{238}U, and ^{40}K activity concentrations, respectively.

Radium equivalent activity (Ra_{eq})

Radium equivalent activity is ascribed to internal as well as external particles of alpha. ^{232}Th, ^{226}Ra, and ^{40}K activity limits are used to manifest the Ra_{eq} index [44,45]:

$$Ra_{eq}\ (Bqkg^{-1}) = Ra + 1.43\ Th + 0.077\ K \quad (2)$$

where Th, Ra, and K are ^{232}Th, ^{226}Ra, and ^{40}K activity concentrations.

Table 4. Variable radiological parameters of Gebel Qulu El Sabaya phosphorites.

S.No	Um	Absorbed nGy/h	Hin	Hex	AED_{out} (mSv)	Ra_{eq} (Bq/kg)	ELCR
1	10.86	223.78	2.69	1.39	0.27	473.88	0.96
2	10	242.51	2.84	1.50	0.30	512.91	1.04
3	10	249.22	2.91	1.54	0.31	549.57	1.07
4	7.71	189.20	2.21	1.17	0.23	413.51	0.81
5	7.71	197.22	2.29	1.22	0.24	474.79	0.85
6	6.86	205.30	2.33	1.26	0.25	481.02	0.88
7	8.29	187.76	2.19	1.15	0.23	442.49	0.81
8	8	218.60	2.52	1.35	0.27	464.14	0.94
9	11.71	239.78	2.90	1.49	0.29	518.28	1.03
10	7.43	167.82	1.97	1.03	0.21	401.96	0.72
11	10.57	218.45	2.63	1.35	0.27	462.78	0.94
12	8.86	221.31	2.57	1.36	0.27	479.85	0.95
13	7.71	189.20	2.21	1.17	0.23	413.51	0.81
14	10.86	239.83	2.86	1.49	0.29	518.73	1.03
15	10.86	231.81	2.78	1.44	0.28	490.76	1.00
Min	7.71	189.20	2.21	1.17	0.23	413.51	0.81
Max	10.86	239.83	2.86	1.49	0.29	518.73	1.03
Av.	9.81	220.28	2.61	1.36	0.27	474.33	0.95
Sd	1.48	22.22	0.29	0.14	0.03	44.50	0.10

Note, Um = Uranium mobilization.

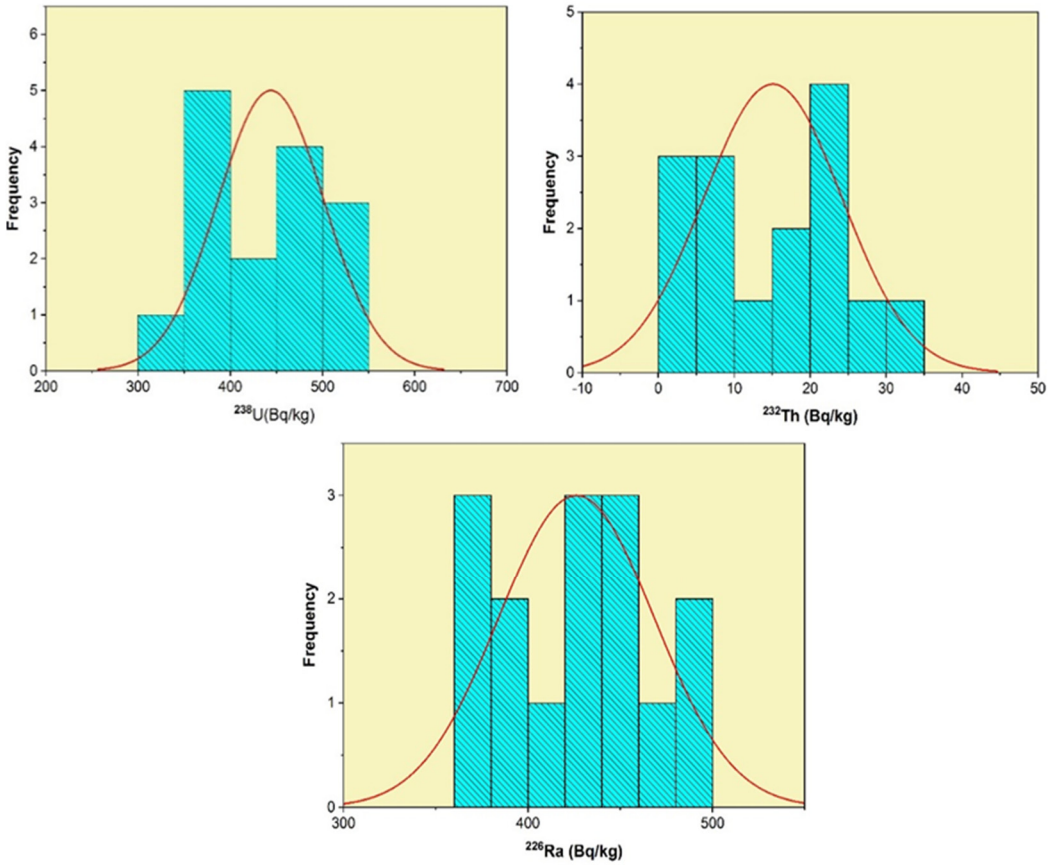

Figure 7. Frequency distribution histograms of ^{238}U, ^{232}Th, and ^{226}Ra activity concentrations, respectively.

Annual effective dose (AED)

Absorbed dose (D_{air}) results, a conversion factor of 0.7 Sv/Gy, indoor and outdoor occupancy factors 0. 8 and 0.2, respectively, are used to estimate AED [46,47]:

$$AED_{out}\ (mSv/y) = D_{air}\ (nGy/h) \times 8.76\ (h) \times 0.2 \times 0.7\ (Sv/Gy) \times 10^{-3} \quad (3)$$

$$AED_{in}\ (mSv/y) = D_{air}\ (nGy/h) \times 8.76\ (h) \times 0.8 \times 0.7\ (Sv/Gy) \times 10^{-3} \quad (4)$$

External and internal radiation indices (H_{ex} &H_{in})

H_{in} and H_{ex} can be measured to infer the radiation effect on human organs. They can be estimated using the following equations [45,48–50]:

$$H_{in} = U/185 + Th/259 + K/4810 \leq 1 \quad (5)$$

$$H_{ex} = U/370 + Th/259 + K/4810 \leq 1 \quad (6)$$

Excess lifetime cancer index (ELCR)

ELCR can be calculated using outdoor annual effective dose, over a lifetime (DL = 70 years) and cancer index (RP = 0.05 Sv) as in this equation:

$$ELCR = AED \times DL \times RP \quad (7)$$

The obtained results of radiological risk parameters (activity concentrations ± standard deviation), including absorbed gamma dose (av. 245 ± 20), annual (outdoor (av. 0.3 ± 0.03) and radium equivalent activity (av. 520 ± 42), external (av. 1.49 ± 0.13) and internal (av. 2.74 ± 28) hazard indices, and excess cancer risk (av. 1.05 ± 0.09) are higher than the acceptable worldwide levels [48], reflecting that the exposure for these deposits for a long time may lead to risk on human organs.

4. Conclusions

The current work discusses stratigraphical, petrographical, radioactivity, and geochemical investigations of the lower phosphorite member of the Gebel Qulu El Sabaya area. It is classified into lower phosphorite (most economical), middle shale, and upper phosphorite members. The former has a total thickness ranging from 2 to 3.5 m and consists of apatite, quartz, hematite, anhydrite, and kaolinite. Geochemically, the lower phosphorite member has high REEs content (av. 1430 ppm), and their patterns reveal a slight negative Eu anomaly. Radiological parameters such as absorbed dose rates, outdoor annual effective dose, radium equivalent activity, external and internal hazard, and excess cancer risk values are higher than the recommended levels, reflecting that exposure to these deposits for a long time may lead to health risks on human organs. Therefore, caution must be taken during the mining of phosphorite or using it as fertilizer.

Author Contributions: Conceptualization, E.S.R.L.; Data curation, E.S.R.L., D.A.S., E.S.R.L., A.E., H.A.A. and H.M.H.Z.; Formal analysis, D.A.S., E.S.R.L., H.A.A. and H.M.H.Z.; Funding acquisition, A.E. and H.M.H.Z.; Investigation, D.F., R.M.E.A., E.S.R.L., H.A.A. and H.M.H.Z.; Methodology, R.M.E.A., E.S.R.L., A.E., H.A.A., B.M.A. and H.M.H.Z.; Project administration, A.E.; Resources, E.S.R.L., B.M.A. and H.M.H.Z.; Software, D.F., R.M.E.A., E.S.R.L., H.A.A. and H.M.H.Z.; Supervision, A.E.; Validation, E.S.R.L., H.A.A. and H.M.H.Z.; Visualization, H.M.H.Z., B.M.A.; Writing—original draft, E.S.R.L., D.A.S., D.F., A.E., H.A.A. and H.M.H.Z.; Writing—review and editing, D.A.S., R.M.E.A., E.S.R.L., A.E., H.A.A., D.F. and H.M.H.Z. All authors have read and agreed to the published version of the manuscript.

Funding: The authors would like to express their gratitude to Princess Nourah bint Abdulrahman University Researchers Supporting Project (grant no. PNURSP2022R32), Princess Nourah bint Abdulrahman University, Riyadh, Saudi Arabia.

Data Availability Statement: The data presented in this study are available on request from the corresponding authors.

Acknowledgments: The authors would like to express their gratitude to Princess Nourah bint Abdulrahman University Researchers Supporting Project (grant no. PNURSP2022R32), Princess Nourah bint Abdulrahman University, Riyadh, Saudi Arabia. The author A.E acknowledges the support of "Dunarea de Jos" University of Galati, Romania.

Conflicts of Interest: The authors declare no conflict of interest.

References

1. Khaleal, F.M.; Saleh, G.M.; Lasheen, E.S.R.; Lentz, D.R. Occurrences and Genesis of Emerald and Other Beryls Mineralization in Egypt: A Review. *Phys. Chem. Earth Parts A B C* **2022**, *128*, 103266. [CrossRef]
2. Saleh, G.M.; Kamar, M.S.; Lasheen, E.S.R.; Ibrahim, I.H.; Azer, M.K. Whole Rock and Mineral Chemistry of the Rare Metals-Bearing Mylonitic Rocks, Abu Rusheid Borehole, South Eastern Desert, Egypt. *J. Afr. Earth Sci.* **2022**, *196*, 104736. [CrossRef]
3. Lasheen, E.S.R.; Saleh, G.M.; Khaleal, F.M.; Alwetaishi, M. Petrogenesis of Neoproterozoic Ultramafic Rocks, Wadi Ibib–Wadi Shani, South Eastern Desert, Egypt: Constraints from Whole Rock and Mineral Chemistry. *Appl. Sci.* **2021**, *11*, 10524. [CrossRef]
4. Hamdy, M.M.; Lasheen, E.S.R.; Abdelwahab, W. Gold-Bearing Listwaenites in Ophiolitic Ultramafics from the Eastern Desert of Egypt: Subduction Zone-Related Alteration of Neoproterozoic Mantle? *J. Afr. Earth Sci.* **2022**, *193*, 104574. [CrossRef]
5. Lasheen, E.S.R.; Mohamed, W.H.; Ene, A.; Awad, H.A.; Azer, M.K. Implementation of Petrographical and Aeromagnetic Data to Determine Depth and Structural Trend of Homrit Waggat Area, Central Eastern Desert, Egypt. *Appl. Sci.* **2022**, *12*, 8782. [CrossRef]
6. Ali, S.; Ntaflos, T.; Sami, M. Geochemistry of Khor Um-Safi Ophiolitic Serpentinites, Central Eastern Desert, Egypt: Implications for Neoproterozoic Arc-Basin System in the Arabian-Nubian Shield. *Geochemistry* **2021**, *81*, 125690. [CrossRef]
7. Abdel-Karim, A.-A.; Azer, M.; Sami, M. Petrogenesis and Tectonic Implications of the Maladob Ring Complex in the South Eastern Desert, Egypt: New Insights from Mineral Chemistry and Whole-Rock Geochemistry. *Int. J. Earth Sci.* **2021**, *110*, 53–80. [CrossRef]
8. Hermina, M.H. Review on the Phosphate Deposits of Egypt. In Proceedings of the Second Arab Conference of Mineral Resources, Santiago, Chile, 13 April–21 May 1972.
9. Issawi, B.; Hassan, M.Y.; Saad, E.N. Geology of Abu Tartur Plateau, Western Desert, Egypt. *Ann. Geol. Surv. Egypt* **1978**, *8*, 91–127.
10. Issawi, B.; El Hinnawi, M.; Francis, M.; Mazhar, A. The Phanerozoic Geology of Egypt. A Geodynamic Approach. Special Publ. No. 76. *Geol. Surv. Cairo Egypt* **1999**, *76*, 462.

11. Fathy, D.; Wagreich, M.; Ntaflos, T.; Sami, M. Provenance Characterization of Campanian Lacustrine Organic-Rich Mudstones on the Southern Tethyan Margin, Egypt. *ACS Earth Space Chem.* **2021**, *5*, 197–209. [CrossRef]
12. Zidan, I.H. *Geological and Mineralogical Studies of Abu Tartur Phosphates, Western Desert-Egypt*; Al-Azhar University: Cairo, Egypt, 1998.
13. Zidan, I.H. *Geological, Mineralogical and Geochemical Studies of Abu Tartur Area. Western Desert, Egypt*; Al Azhar University: Cairo, Egypt, 2002.
14. Zidan, I.H. Evaluation of Phosphorite and Uranium in Lower Member, Duwi Formation at Kummer Area South Esna, West Nile Valley, Egypt. *J. Sedimentol. Soc. Egypt* **2013**, *21*, 143–154.
15. Jarvis, I.; Burnett, W.; Nathan, Y. Phosphorite Geochemistry: State-of-the-Art and Environmental Concerns. *Eclogae Geol. Helv.* **1994**, *87*, 643–700.
16. Slansky, M. *Geology of Sedimentary Phosphates*; Originally Published in French in 1980; Cambridge University Press: Cambridge, UK, 2009. [CrossRef]
17. Amin, M.M.; Zidan, I.H. Rare Earth Elements Recovery and Preparation of Phosphoric Acid from Abu-Tartur Phosphate Rock Using Penicillium Simplicissimum. *Chem. Technol. Indian J.* **2014**, *10*, 57–61.
18. Ilyin, A.V. Rare-Earth Geochemistry of "old" Phosphorites and Probability of Syngenetic Precipitation and Accumulation of Phosphate. *Chem. Geol.* **1998**, *144*, 243–256. [CrossRef]
19. Hannigan, R.E.; Sholkovitz, E.R. The Development of Middle Rare Earth Element Enrichments in Freshwaters: Weathering of Phosphate Minerals. *Chem. Geol.* **2001**, *175*, 495–508. [CrossRef]
20. Zakaly, H.M.; Uosif, M.A.; Madkour, H.; Tammam, M.; Issa, S.; Elsaman, R.; El-Taher, A. Assessment of Natural Radionuclides and Heavy Metal Concentrations in Marine Sediments in View of Tourism Activities in Hurghada City, Northern Red Sea, Egypt. *J. Phys. Sci.* **2019**, *30*, 21–47. [CrossRef]
21. Zidan, I.H. Evaluation of Phosphorite and Uranium Resources of Duwi Formation at Helal Area, South Esna, East Nile Valley, Egypt. *Sedimentol. Egypt* **2017**, *23*, 63–80.
22. Negm, S.H. *Mineralogical and Geochemical Studies of the Duwi Formation Phosphatic Rock in El-Sibaiya. East Area. Nile Vally Egypt*; Minufiya University: Al Minufiyah, Egypt, 2009.
23. Altschuler, Z.A. The Geochemistry of Trace Elements in Marine Phosphorites, Part I. Characteristic Abundances and Enrichment. In *Marine Phosphorites*; The Society for Sedimentary Geology: Tulsa, OK, USA, 1980; pp. 19–30. [CrossRef]
24. El-Kammar, A. *Comparative Geochemical and Mineralogical Studies on Egyptian Phosphorites*; Cairo University: Cairo, Egypt, 1974.
25. Dardir, A.A.; Kobtan, S.M. Preliminary Evaluation of the Rare-Earth Elements in Sector Abu Tartur Phosphorites. *Ann. Geol. Surv. Egypt* **1980**, *10*, 909–921.
26. El-Sankary, M.; Mahdy, A. The Heavy Minerals Associating Phosphorites of the Western Desert of Egypt: Possible Supplier of Trace Elements and provenance indicator. In Proceedings of the 7th International Conference on Geochemistry, Alexandria, Egypt, 6–7 September 2006; Volume II, pp. 15–30.
27. Taylor, S.R.; McLennan, S.M. *The Continental Crust: Its Composition and Evolution*; U.S. Department of Energy: Germantown, MD, USA, 1985.
28. El-Kammar, A.; El-Kammar, M. On the Trace Elements Composition of the Egyptian Phosphorites: A New Approach. In Proceedings of the 6th International Conference on the Geology of the Arab World, Giza, Egypt, 21–24 February 2002; Cairo University: Cairo, Egypt, 2002; pp. 227–244.
29. Elderfield, H.; Greaves, M.J. The Rare Earth Elements in Seawater. *Nature* **1982**, *296*, 214–219. [CrossRef]
30. Kolodny, Y. Phosphorite. In *Encyclopedia of Paleoclimatology and Ancient Environments*; Gornitz, V., Ed.; Encyclopedia of Earth Sciences Series; Springer: Dordrecht, The Netherlands, 2009. [CrossRef]
31. McArthur, J.M.; Walsh, J.N. Rare-Earth Geochemistry of Phosphorites. *Chem. Geol.* **1984**, *47*, 191–220. [CrossRef]
32. De Baar, H.J.W.; Bacon, M.P.; Brewer, P.G.; Bruland, K.W. Rare Earth Elements in the Pacific and Atlantic Oceans. *Geochim. Cosmochim. Acta* **1985**, *49*, 1943–1959. [CrossRef]
33. Piper, D.; Baedecker, P.; Crock, J.; Geology, W.B.-M. *Undefined Rare Earth Elements in the Phosphatic-Enriched Sediment of the Peru Shelf*; Elsevier: Amsterdam, The Netherlands, 1988.
34. Bonnot-Courtois, C.; Flicoteaux, R. Distribution of Rare-Earth and Some Trace Elements in Tertiary Phosphorites from the Senegal Basin and Their Weathering Products. *Chem. Geol.* **1989**, *75*, 311–328. [CrossRef]
35. El Gemmizi, M.A.; Ali, M.M. Contribution of heavy minerals to the trace elements from East Sebaiya phosphorites, Egypt. Proc. 2nd Int. Conf. Geol. Arab World, Cairo Univ. 1999, 145-153.
36. Hassan, F.; El-Kammar, A. Environmental Conditions Affecting the Distribution of Uranium and Rare Earth Elements in Egyptian Phosphorites. *Egypt. J. Pet.* **1975**, *19*, 169–178.
37. Lucas, J.; Flicoteaux, R.; Nathan, Y.; Prevot, L.; Shahar, Y. Different Aspects of Phosphorite Weathering. In *Marine Phosphorites*; The Society for Sedimentary Geology: Tulsa, OK, USA, 1980; pp. 41–51. [CrossRef]
38. Guirgues, N.R. *Geological and Geochemical Studies on Some Phosphate Exposures, East-Central Sinai, Egypt*; Mansoura University: Mansoura, Egypt, 2005.
39. Hussein, A.H. *Lecture Course in Nuclear Geology*; NMA Egypt; Ain Shams University: Cairo, Egypt, 1978; 101p.
40. Hansink, J.D. Equilibrium Analysis of a Sandstone Roll-Front Uranium Deposit. 1976. Available online: https://inis.iaea.org (accessed on 20 August 2022).

41. Wignall, P.B.; Myers, K.J. Interpreting Benthic Oxygen Levels in Mudrocks: A New Approach. *Geology* **1988**, *16*, 452–455. [CrossRef]
42. UNSCEAR. *Sources and Effects of Ionizing Radiation*; UNSCEAR 2000 Report to the General Assembly, with Scientific Annexes; United Nations Scientific Committee on the Effects of Atomic Radiation: Vienna, Austria, 2000; ISBN 92-1-142238-8.
43. UNSCEAR. *Sources and Effects of Ionizing Radiation*; United Nations Scientific Committee on the Effects of Atomic Radiation: Vienna, Austria, 2008; Volume 1, ISBN 9789211422740.
44. Ravisankar, R.; Chandramohan, J.; Chandrasekaran, A.; Prince Prakash Jebakumar, J.; Vijayalakshmi, I.; Vijayagopal, P.; Venkatraman, B. Assessments of Radioactivity Concentration of Natural Radionuclides and Radiological Hazard Indices in Sediment Samples from the East Coast of Tamilnadu, India with Statistical Approach. *Mar. Pollut. Bull.* **2015**, *97*, 419–430. [CrossRef]
45. Kamar, M.S.; Salem, I.A.; El-Aassy, I.E.; El-Sayed, A.A.; Zakaly, H.M.H.; Alzahrani, A.M.; Saeed, E.; Lasheen, R. An Extended Investigation of High-Level Natural Radioactivity and Geochemistry of Neoproterozoic Dokhan Volcanics: A Case Study of Wadi Gebeiy, Southwestern Sinai, Egypt. *Sustainability* **2022**, *14*, 9291. [CrossRef]
46. Abbasi, A. Calculation of Gamma Radiation Dose Rate and Radon Concentration Due to Granites Used as Building Materials in Iran. *Radiat. Prot. Dosim.* **2013**, *155*, 335–342. [CrossRef]
47. Zakaly, H.M.H.; Uosif, M.A.M.; Issa, S.A.M.; Tekin, H.O.; Madkour, H.; Tammam, M.; El-Taher, A.; Alharshan, G.A.; Mostafa, M.Y.A. An Extended Assessment of Natural Radioactivity in the Sediments of the Mid-Region of the Egyptian Red Sea Coast. *Mar. Pollut. Bull.* **2021**, *171*, 112658. [CrossRef]
48. UNSCEAR. *2008 Sources and Effects of Ionising Radiation*; Report to the General Assembly with Scientific Annexes; UNSCEAR: New York, NY, USA, 2010.
49. Lasheen, E.S.R.; Azer, M.K.; Ene, A.; Abdelwahab, W.; Zakaly, H.M.H.; Awad, H.A.; Kawady, N.A. Radiological Hazards and Natural Radionuclide Distribution in Granitic Rocks of Homrit Waggat Area, Central Eastern Desert, Egypt. *Materials* **2022**, *15*, 4069. [CrossRef]
50. Alharshan, G.A.; Kamar, M.S.; Lasheen, E.S.R.; Ene, A.; Uosif, M.A.M.; Awad, H.A.; Issa, S.A.M.; Zakaly, H.M.H. Distribution of Radionuclides and Radiological Health Assessment in Seih-Sidri Area, Southwestern Sinai. *Int. J. Environ. Res. Public. Health* **2022**, *19*, 10717. [CrossRef] [PubMed]